Theoretical and Experimental Characterization of Coplanar Waveguide Discontinuities for Filter Applications

Nihad I. Dib, *Student Member, IEEE*, Linda P. B. Katehi, *Senior Member, IEEE*, George E. Ponchak, *Member, IEEE*, and Rainee N. Simons, *Senior Member, IEEE*

Abstract —A full-wave analysis of shielded coplanar waveguide two-port discontinuities based on the solution of an appropriate surface integral equation in the space domain is presented. Using this method, frequency-dependent scattering parameters for open-end and short-end CPW stubs are computed. The numerically derived results are compared with measurements performed in the frequency range 5–25 GHz and show very good agreement. Equivalent circuit models and closed-form expressions to compute the circuit element values for these discontinuities are also presented.

I. INTRODUCTION

RECENTLY, coplanar waveguide (CPW) technology has attracted a great deal of interest for RF circuit design owing to several advantages over the conventional microstrip line, among them the capability to wafer probe at millimeter-wave frequencies [1]–[6]. Thus, several investigators have undertaken the study of the propagation characteristics of uniform CPW, and extensive data are available in the literature [7]. However, very few models are available on CPW discontinuities, which are useful in the design of circuits such as filters [8]–[12].

Filters are important blocks in microwave circuits and are among the first few circuit elements studied in any new technology. Microstrip or stripline filters have been extensively studied and very accurate design techniques have been presented in the literature [13]. However, CPW filter elements [1], [14] have been investigated only experimentally and lack accurate equivalent circuits. Two such filter elements are the short-end and open-end series stubs, which are shown in Fig. 1(a) and (b) respectively. In this figure *PP'* refers to the reference planes, which are coincident with the input and output ports of the discontinuity. The short-end CPW stub was modeled by Houdart [1] as a series inductor. This model cannot predict the

resonant nature of the stub as it approaches $\lambda_g/4$ or the asymmetry of the discontinuity; therefore, it is valid only in the limit as the stub length approaches zero. The model used by Ponchak and Simons [15], an ideal short-end series stub, predicts the resonant nature of the stub but not the asymmetry. The open-end CPW stub was modeled by Houdart [1] as a series capacitor, which is also too simple to predict the resonant nature of the stub or its asymmetry and is valid only for stubs with very small lengths. Williams [14] expanded this model to a capacitive Π network and selected a reference plane which removed the element asymmetry. This improved model is difficult to incorporate into CAD programs since the reference planes are not at the plane of the discontinuity, as shown in Fig. 1. The model by Ponchak and Simons [15], an ideal open-end series stub, again cannot predict the element asymmetry.

This paper attempts, for the first time, to study theoretically and experimentally the two CPW filter elements shown in Fig. 1. The theoretical method used to study these CPW discontinuities is based on a space-domain integral equation (SDIE), which is solved using the method of moments [16]. The main difference between this approach and the one used in [3] and [10]–[12] is that the boundary conditions are applied in the space domain instead of the spectral domain. Thus, in the SDIE method the Fourier transforms of the basis functions, which are used in the method of moments, are not required, which makes it simpler to handle complicated geometries. The SDIE approach has previously been applied to study several CPW discontinuities and has shown very good accuracy, efficiency, and versatility in terms of the geometries it can solve [17], [18]. Using this method, theoretical results for the scattering parameters of the two CPW discontinuities shown in Fig. 1 are computed. Extensive experiments have been performed in the frequency range 5 to 25 GHz to validate the theoretically derived scattering parameters, and a very good agreement has been found. From the scattering parameters, lumped element equivalent circuits have been derived to model the discontinuities. The inductors and capacitors of these models have been represented by closed-form equations, as functions of the stub length, which have potential applications
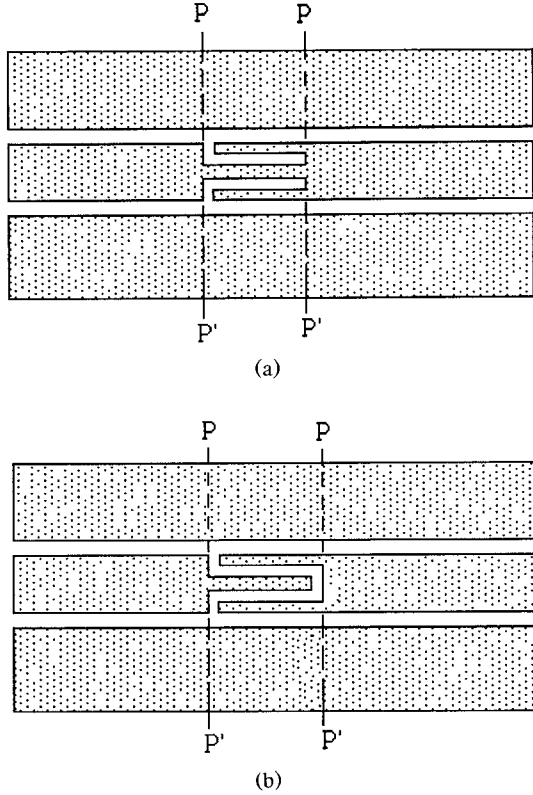
(a)

(b)

Fig. 1.   Coplanar waveguide filter elements. (a) Short-end CPW series
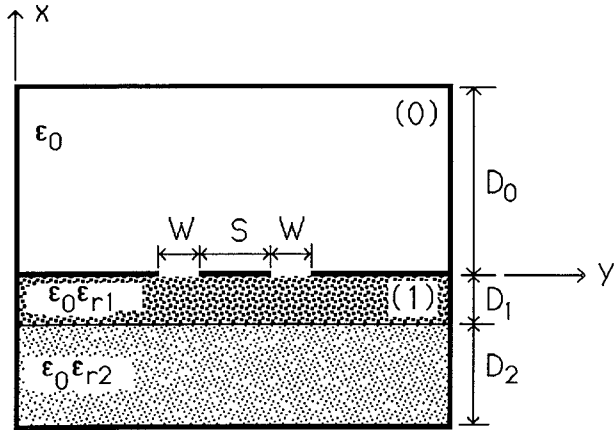stub. (b) Open-end CPW series stub.

Fig. 2.   A cross section of a shielded CPW.

in the design of CPW circuits. In addition, these circuits
are capable of modeling the ON and OFF states of CPW
p-i-n diode switches [15].

II. THEORY

A. Derivation of the Scattering Parameters

Fig. 2 shows a shielded coplanar waveguide with the
cavity dimensions chosen such that the CPW fundamental
mode is not affected by higher order cavity resonances.
The original boundary problem is divided into two sim-
pler ones by introducing an equivalent magnetic current,
$\vec{M}_s$, on the slot aperture (see the Appendix). This surface

magnetic current radiates an electromagnetic field in the
two waveguide regions (above and below the slots) so that
the continuity of the electric field on the surface of the
slots is satisfied. The remaining boundary condition to be
applied is the continuity of the tangential components of
the magnetic field on the surface of the slot aperture,

$$\hat{a}_x \times \left(\vec{H}_0 - \vec{H}_1 \right) = \vec{J}_s \tag{1}$$

where $\vec{J}_s$ vanishes everywhere on the plane of the slot
apertures except at the position of the electric current
sources exciting the CPW. $\vec{H}_{0,1}$ are the magnetic fields in
the regions directly above and below the slot aperture,
respectively (see Fig. 12), and can be expressed in terms
of the equivalent magnetic current density, $\vec{M}_s$, as shown
below:

$$\vec{H}_0 = \int_{S_{CPW}} \int \overline{\overline{G}}_0^h (\vec{r}/\vec{r}') \cdot \vec{M}_s(\vec{r}') \, ds' \tag{2}$$

$$\vec{H}_1 = - \int_{S_{CPW}} \int \overline{\overline{G}}_1^h (\vec{r}/\vec{r}') \cdot \vec{M}_s(\vec{r}') \, ds'. \tag{3}$$

In (2) and (3), S_{CPW} is the surface of the slot aperture,
and $\overline{\overline{G}}_{0,1}^h$ is the dyadic Green's function in the two wave-
guide regions (see the Appendix).

In view of (2) and (3), (1) takes the form

$$\hat{a}_x \times \int_{S_{CPW}} \int \left[\overline{\overline{G}}_0^h + \overline{\overline{G}}_1^h \right] \cdot \vec{M}_s(\vec{r}') \, ds' = \vec{J}_s. \tag{4}$$

To obtain the unknown magnetic current distribution,
$\vec{M}_s$, (4) is solved by applying the method of moments [16].
First, the slot aperture is subdivided into rectangles. Then,
the unknown magnetic current density is expressed as a
finite double summation:

$$\vec{M}_s(\vec{r}') = \hat{a}_y \sum_{i=1}^{N_y} \sum_{j=1}^{N_z} V_{y,ij} f_i(y') g_j(z')$$

$$+ \hat{a}_z \sum_{i=1}^{N_y} \sum_{j=1}^{N_z} V_{z,ij} f_j(z') g_i(y') \tag{5}$$

where $\{f_i(y') g_j(z'); i = 1, \cdots, N_y, j = 1, \cdots, N_z\}$ is a family
of rooftop functions [19] and $V_{y,ij}$ and $V_{z,ij}$ are the un-
known coefficients for the y and z components of the
magnetic current density. The subdomain basis functions
(rooftop functions) for each current component have
piecewise-sinusoidal variation along the longitudinal di-
rection and constant variation along the transverse direc-
tion. Using (5), (4) can be written in the form

$$\vec{J}_s + \Delta \vec{J}_s = \hat{a}_x \times \left\{ \sum_{i=1}^{N_y} \sum_{j=1}^{N_z} V_{y,ij} \int \int \left[\overline{\overline{G}}_0^h + \overline{\overline{G}}_1^h \right] \right.$$

$$\cdot \hat{a}_y f_i(y') g_j(z') \, ds'$$

$$+ \sum_{i=1}^{N_y} \sum_{j=1}^{N_z} V_{z,ij} \int \int \left[\overline{\overline{G}}_0^h + \overline{\overline{G}}_1^h \right]$$

$$\left. \cdot \hat{a}_z f_j(z') g_i(y') \, ds' \right\} \tag{6}$$

where $\Delta \vec{J}_s$ represents the error introduced from the ap-

proximations made in the magnetic current distribution (eq. (5)).

Finally, Galerkin's procedure is used to minimize the error $\Delta \vec{J_s}$ resulting in the following inner products:

$$\iint \left(\hat{a}_x \times \Delta \vec{J_s} \right) \cdot \hat{a}_y f_m(y) g_n(z)\, ds = 0 \qquad (7)$$

$$\iint \left(\hat{a}_x \times \Delta \vec{J_s} \right) \cdot \hat{a}_z f_n(z) g_m(y)\, ds = 0 \qquad (8)$$

where f_m and g_n are weighting functions identical to the basis functions, $m = 1, \cdots, N_y$ and $n = 1, \cdots, N_z$. In this manner, (6) reduces into a matrix equation of the form

$$\begin{pmatrix} [Y_{yy}] & [Y_{yz}] \\ [Y_{zy}] & [Y_{zz}] \end{pmatrix} \begin{pmatrix} V_y \\ V_z \end{pmatrix} = \begin{pmatrix} I_z \\ I_y \end{pmatrix} \qquad (9)$$

where $[Y_{\zeta\xi}]$ ($\zeta, \xi = y, z$) represent blocks of the admittance matrix whose elements are expressed in terms of multiple space integrals, involving trigonometric functions, and are given by

$$Y_{yy} = \iiiint \hat{a}_y f_m(y) g_n(z) \cdot \left[\overline{\overline{G}}_0^h + \overline{\overline{G}}_1^h \right]$$
$$\cdot \hat{a}_y f_i(y') g_j(z')\, dy' dz'\, dy\, dz \qquad (10)$$

$$Y_{yz} = \iiiint \hat{a}_y f_m(y) g_n(z) \cdot \left[\overline{\overline{G}}_0^h + \overline{\overline{G}}_1^h \right]$$
$$\cdot \hat{a}_z f_j(z') g_i(y')\, dy' dz'\, dy\, dz \qquad (11)$$

$$Y_{zy} = \iiiint \hat{a}_z f_n(z) g_m(y) \cdot \left[\overline{\overline{G}}_0^h + \overline{\overline{G}}_1^h \right]$$
$$\cdot \hat{a}_y f_i(y') g_j(z')\, dy' dz'\, dy\, dz \qquad (12)$$

$$Y_{zz} = \iiiint \hat{a}_z f_n(z) g_m(y) \cdot \left[\overline{\overline{G}}_0^h + \overline{\overline{G}}_1^h \right]$$
$$\cdot \hat{a}_z f_j(z') g_i(y')\, dy' dz'\, dy\, dz \qquad (13)$$

where $i, m = 1, \cdots, N_y$ and $j, n = 1, \cdots, N_z$. V_y and V_z are the subvectors of the unknown coefficients for the y and z components of the magnetic current distribution respectively and I_y and I_z are the known excitation subvectors, which are dependent on the impressed feed model.

In order to solve (9), the excitation is modeled by ideal y-directed current sources located at specific node points, as shown in Fig. 3(a), resulting in an excitation vector which has zeros everywhere except at the positions of these current sources (delta gap current generators). Although only a mathematical model, this feeding mechanism has proved to be efficient, accurate, and reliable [17], [20]. In addition, it does not introduce any unwanted numerical complications, as is the case with other excitation techniques [3], [12]. The CPW may be excited in two different ways: with the fields on the two slot apertures in phase (slotline mode) or out of phase (coplanar mode), exhibiting very different characteristics when operating in each mode. The CPW mode is excited by choosing $I'_{g1} = -I_{g1}$ and $I'_{g2} = -I_{g2}$, while the slotline mode is excited by choosing $I'_{g1} = I_{g1}$ and $I'_{g2} = I_{g2}$ (see Fig. 3(a)). However, only the CPW mode will be considered here since it tends to concentrate the fields around the slot aperture
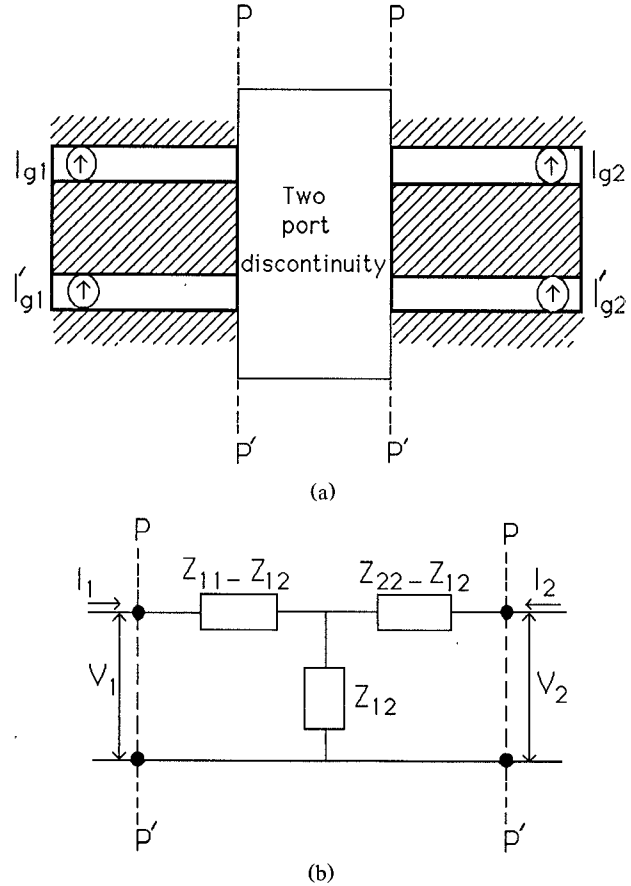

Fig. 3. (a) A general two-port CPW discontinuity with y-directed electric current sources. (b) Equivalent network representation.

(low radiation losses) and is therefore the commonly used mode in CPW circuits.

The discontinuities behave as an asymmetric two-port network with an equivalent circuit of the type shown in Fig. 3(b). For the evaluation of the network impedance matrix, three different modes of excitation are required ($I_{g1} = I_{g2} = 1$, $I_{g1} = -I_{g2} = 1$, and $I_{g1} = 1$ and $I_{g2} = 0$ were used). It should be noticed that the currents and voltages (I_1, I_2, V_1, V_2) shown in Fig. 3(b) are induced at the discontinuity ports as a consequence of I_{g1} and I_{g2}. The matrix equation (9) is solved to give the magnetic current distribution in the slot aperture for each mode of excitation. Then, the input impedances at ports 1 and 2 are evaluated from the positions of the minima and the maxima of the electric field standing waves in the feeding CPW lines using ideal transmission line theory. Finally, the network impedance matrix and the scattering parameters are derived using the expressions in [21].

B. Convergence Properties of Scattering Parameters

In the expressions for the Green's functions given in the Appendix, the summations over m and n are theoretically infinite. However, for the numerical solution of the matrix equation, these summations are truncated to MSTOP and NSTOP. The values of these two parameters should be chosen such that convergence of the scattering coeffi-
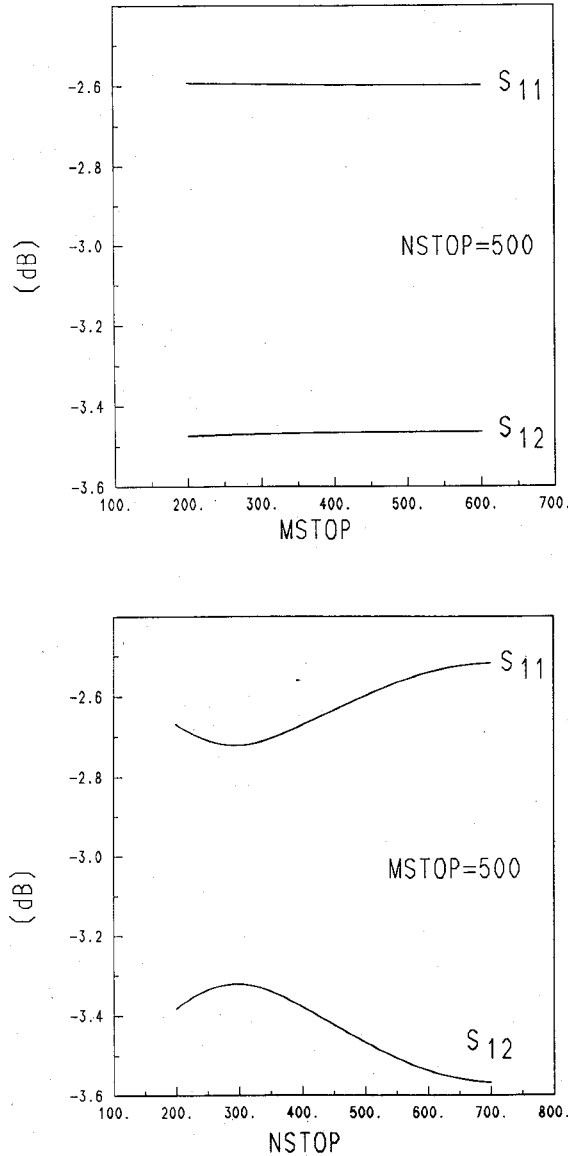
Fig. 5. The assumed magnetic current distribution in the slot aperture.

Transition regions where both y- and z-directed magnetic currents are assumed.

and N_z. Since the slots are assumed to be fairly thin $(W / \lambda_{\mathrm{CPW}} < 0.1)$, only a longitudinal magnetic current in the slot aperture away from the discontinuity is assumed. Furthermore, it has been found through numerical experiments that the transverse current in the feeding line around the discontinuity has a negligible effect on the current distribution and the scattering parameters. Thus, as shown in Fig. 5, both longitudinal and transverse magnetic current components are considered in the transition regions, while only the longitudinal current component is considered in the other regions. In addition, the number of basis functions N_y and N_z is chosen so that convergence of the scattering parameters of the coplanar waveguide discontinuity is achieved. The CPU time required for the evaluation of the scattering parameters depends mainly on the geometry and the electrical size of the structure. Careful consideration of the existing physical symmetries can reduce this computational time substantially.

Fig. 4. Typical convergence behavior of the scattering parameters with respect to the number of modes NSTOP and MSTOP of the CPW discontinuities shown in Fig. 1.

cients is ensured. Fig. 4 shows the convergence behavior of the scattering coefficients with respect to each one of the above parameters. In (A10)–(A13), NSTOP and MSTOP correspond to the maximum values of the k_z and k_y eigenvalues considered in the summations. These eigenvalues are given by

$$k_{z \max} = \frac{(\text{NSTOP}) \pi}{l} \qquad (14)$$

$$k_{y \max} = \frac{(\text{MSTOP}) \pi}{a}. \qquad (15)$$

Since the length of the cavity, l, is larger than its width, a, the number of required k_z eigenvalues (NSTOP = 700) is much larger than the number of k_y eigenvalues (MSTOP = 300), as shown in Fig. 4.

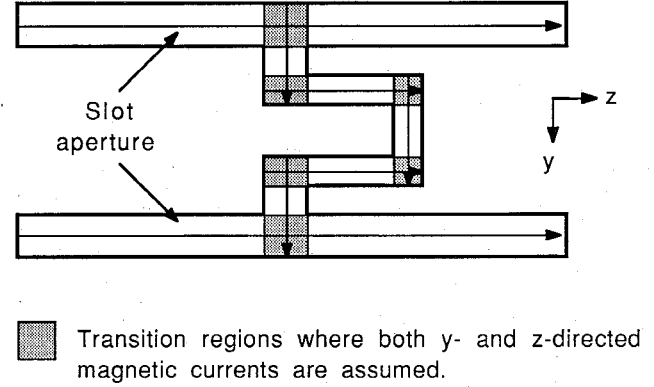Another critical parameter for the convergence of the results is the number of the considered basis functions N_y

III. RESULTS AND DISCUSSION

Using the space-domain integral equation method, the scattering parameters for the two discontinuities shown in Fig. 1 have been evaluated as a function of the stub length, L, and frequency. The theoretically derived data have been validated through extensive experiments performed in the 5 through 25 GHz frequency range. The circuits were fabricated using conventional MIC techniques on a polished alumina $(\epsilon_r = 9.9)$ substrate. The plated gold thickness was 2.8 μm. The RF measurements were performed on an HP 8510 ANA. A probe station with dc–26.5 GHz probes was used for providing the RF connections to the circuits. A two-tier calibration was performed: First, the system was calibrated to the 3.5 mm coaxial cable ends using coaxial open, short, load calibration standards. Then, an LRL calibration was performed to rotate the reference planes to the CPW discontinuities. The LRL calibration standards shown in Fig. 6 were fabricated on the substrate along with the circuits to eliminate errors caused by fabrication nonrepeatability. Air bridges were not needed to connect the ground planes since the discontinuities considered here are symmetric
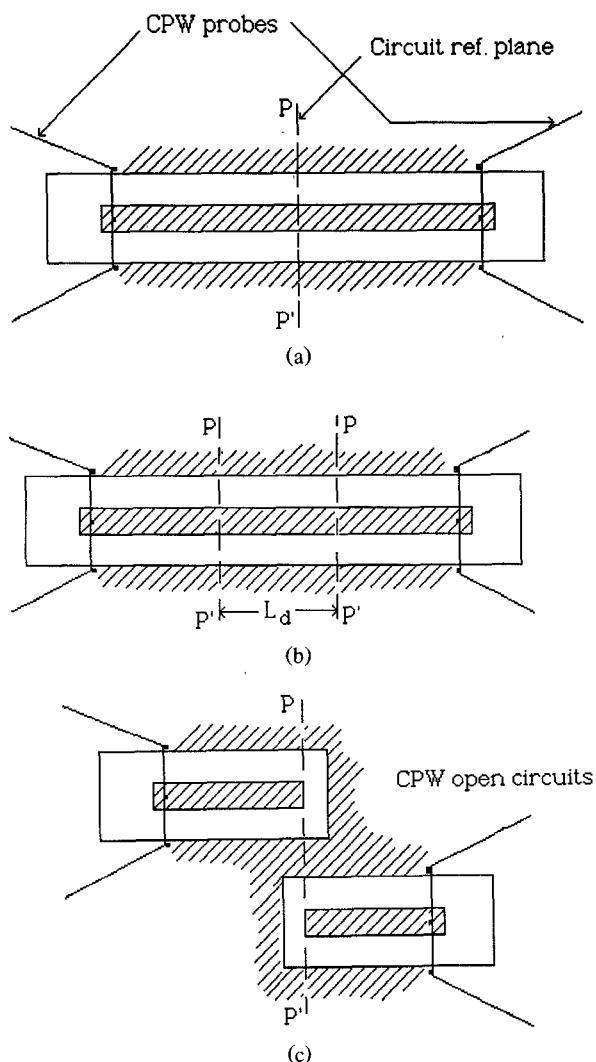
Fig. 6. CPW standards for LRL calibration: (a) Zero length thru line. (b) Delay of length L_d where $0 \leqslant L_d \leqslant \lambda/2$. (c) Open circuit reflection standards.

Fig. 7. Scattering parameters for the short-end CPW stub with $L = 1500$ μm ($D_1 = 25$ mil, $D_2 = 125$ mil, $\epsilon_{r1} = 9.9$, $\epsilon_{r2} = 2.2$; other dimensions are in μm).

about the propagation line, and the stubs are printed on the center conductor [22]. The alumina substrate was placed on a 125-mil-thick 5880 RT/Duroid ($\epsilon_r = 2.2$) substrate with copper cladding on one side to serve as the bottom ground plane.

Fig. 7 shows the scattering parameters for the short-end CPW stub of length 1500 μm. It can be seen that the agreement between the theoretical and experimental results is very good. The differences are due to radiation, conductor, and dielectric losses since an unshielded structure was used in the measurements and the theoretical model did not account for losses. From the characteristic behavior of the above stub, it can be concluded that a band-stop filter can be realized by cascading several of these stubs in series.

Fig. 8 shows a comparison between theoretical and experimental values of the resonant frequency as a function of stub length. In addition, superimposed are values of the resonant frequencies for the above CPW stub operating under ideal conditions: no discontinuity effects and zero electromagnetic interactions. It can be noticed
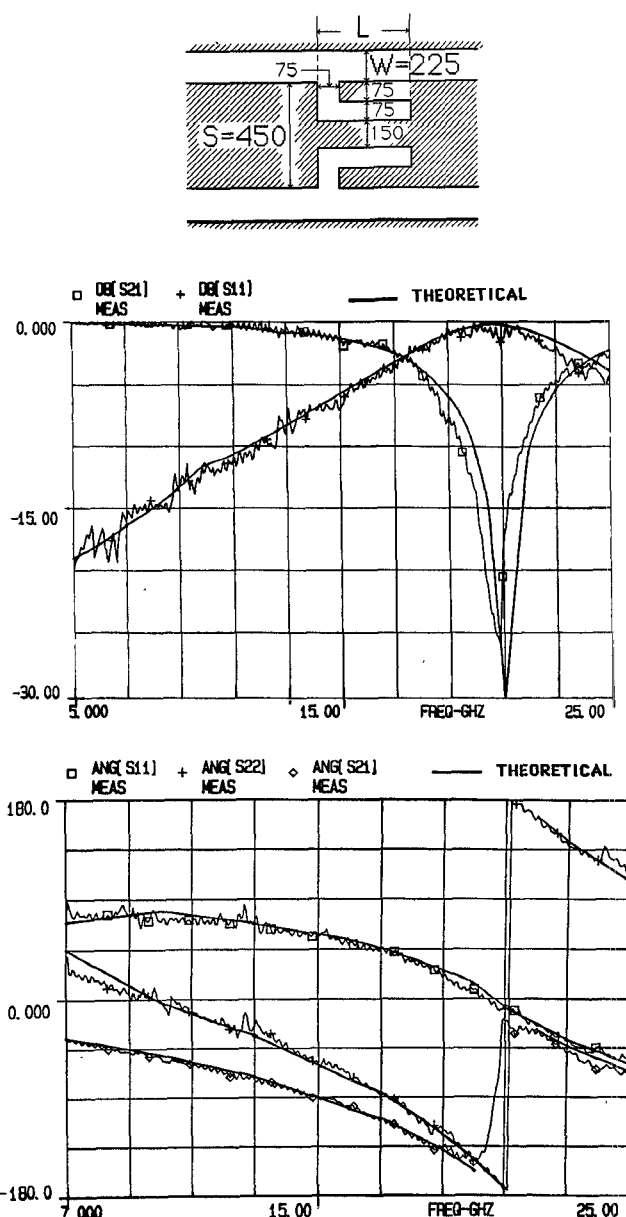
that the theoretically computed resonant frequencies for large stub lengths agree very well with the ones predicted for the ideal stub. This indicates that at low resonant frequencies (large stub lengths) the specific stub geometry introduces negligible discontinuity effects and is almost free of parasitic electromagnetic interactions. However, as the frequency increases, the parasitic effects become stronger, resulting in a small difference between the theoretically obtained resonant frequencies and the ones computed for the ideal stub.

Fig. 9 shows the scattering parameters for the open-end CPW stub of length 1500 μm. As in the previous case, the agreement between the theoretical and experimental results is very good. Owing to its performance, such structures can be used to build band-pass filters.
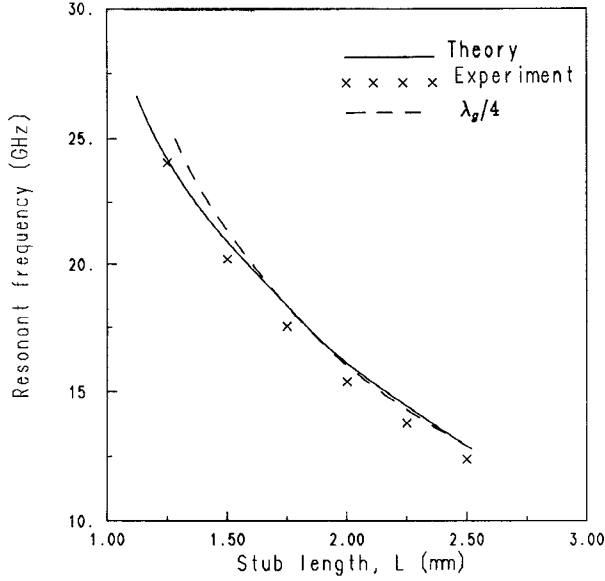
Fig. 8. Resonant frequency of the short-end CPW stub of different lengths ($D_1 = 21.5$ mil. $D_2 = 125$ mil, $\epsilon_{r1} = 9.9$, $\epsilon_{r2} = 2.2$; other dimensions are as in Fig. 10(a)).

In the theoretical analysis, the CPW stubs were assumed to be inside a cavity while for the derivation of experimental data these structures were measured in open environment. The fact that there is very good agreement between theory and experiment suggests that radiation losses were very low. The loss factor of the measured stub discontinuities has been investigated and has shown a maximum value of -10 dB at the stub's resonant frequency. This indicates that it is possible to design CPW stub discontinuities with very low radiation losses.

IV. EQUIVALENT MODELS

To accurately model the short-end CPW stub over the frequency range from 5 GHz to the first band-stop resonance, the model shown in Fig. 10(b) is proposed. Using the derived scattering parameters (for Fig. 10(a)), the capacitances and inductances are evaluated using commercial optimization software. The following relations have been found, which give the values of the lumped elements in terms of the stub length, L:

$$C_s = 1.32 \times 10^{-4} L + 3.3515 \times 10^{-2} \qquad (16)$$

$$C_{f1} = 1.5959 \times 10^{-2} \qquad (17)$$

$$C_{f2} = 1.1249 \times 10^{-4} L + 7.522 \times 10^{-3} \qquad (18)$$

$$L_1 = 2.6368 \times 10^{-4} L - 6.618 \times 10^{-3} \qquad (19)$$

$$L_2 = 1.77 \times 10^{-4} L - 8.35 \times 10^{-4} \qquad (20)$$

$$L_3 = 1.8656 \times 10^{-4} L - 8.34 \times 10^{-4} \qquad (21)$$

where the stub length, L, is in μm, the inductances in nH, and the capacitances in pF. The above equations, which apply for the configuration shown in Fig. 10(a) only, have been verified for stub lengths, L, through 2500 μm. It should be noted that $C_{f1} = C_{f2}$ and $L_1 = L_3$ when
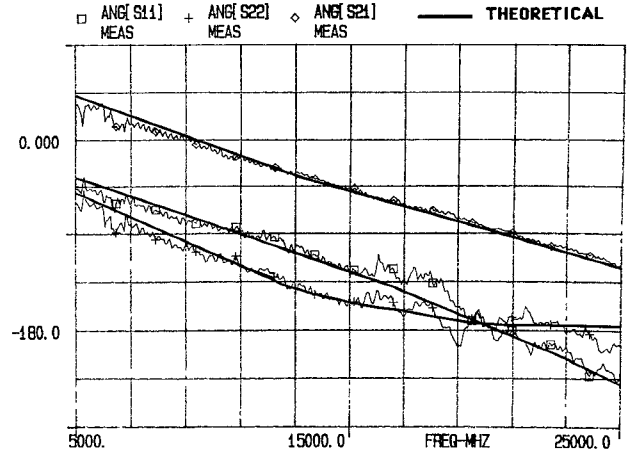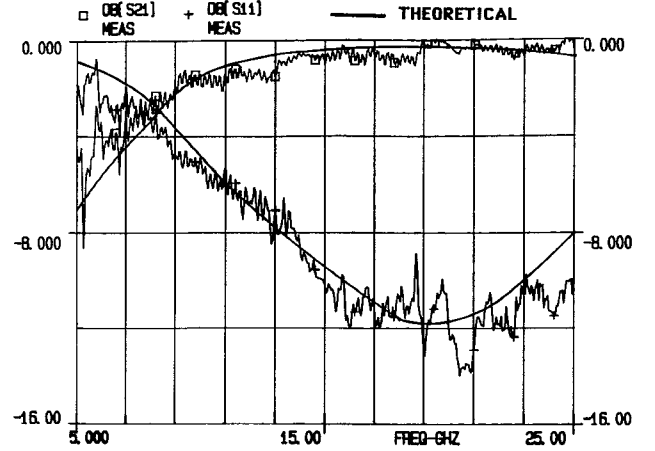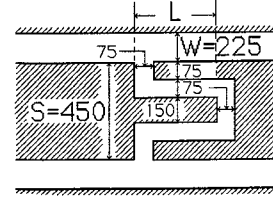

Fig. 9. Scattering parameters for the open-end CPW stub with $L = 1500$ μm ($D_1 = 25$ mil, $D_2 = 125$ mil, $\epsilon_{r1} = 9.9$, $\epsilon_{r2} = 2.2$; other dimensions are in μm).

$L = 75$ μm since a symmetric model is expected for a simple notch in the center conductor of the CPW.

The equivalent circuit shown in Fig. 11(b) is proposed to model the open-end CPW stub over the frequency range from 5 GHz to the first band-pass resonance. The following relations have been found, which give the values of the lumped elements in terms of the stub length, L:

$$C_s = 1.01 \times 10^{-4} L + 1.642 \times 10^{-2} \qquad (22)$$

$$C_{f1} = 0.39 \times 10^{-4} L + 1.765 \times 10^{-2} \qquad (23)$$

$$C_{f2} = 0.883 \times 10^{-4} L + 1.765 \times 10^{-2} \qquad (24)$$

$$L_1 = 1.22 \times 10^{-4} L \qquad (25)$$

$$L_2 = 1.43 \times 10^{-4} L \qquad (26)$$

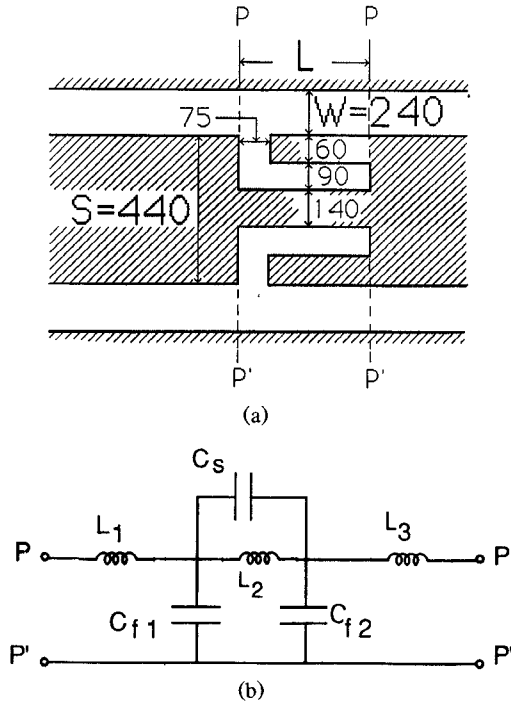$$L_3 = 3.26 \times 10^{-4} L \qquad (27)$$

(a)

(b)

Fig. 10. Equivalent circuit for the short-end CPW stub ($D_1 = 21.5$ mil, $D_2 = 125$ mil, $\epsilon_{r1} = 9.9$, $\epsilon_{r2} = 2.2$; other dimensions are in μm).
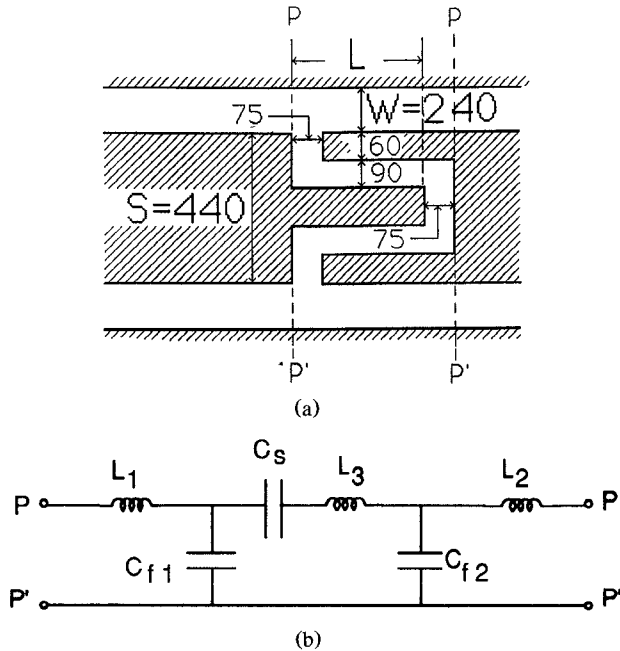

(a)

(b)

Fig. 11. Equivalent circuit for the open-end CPW stub ($D_1 = 21.5$ mil, $D_2 = 125$ mil, $\epsilon_{r1} = 9.9$, $\epsilon_{r2} = 2.2$; other dimensions are in μm).

where the stub length, L, is in μm, the inductances in nH, and the capacitances in pF. As in the previous case, the above equations, which apply for the configuration shown in Fig. 11(a) only, have been verified for stub lengths, L, through 2500 μm. In the limit as L approaches zero, the inductances reduce to zero and C_{f1} becomes equal to C_{f2}, resulting in a capacitive Π network which is expected for a series gap.

The above lumped element equivalent circuits predict the response up to the first resonant frequency with a 5% accuracy. It is expected that similar linear relationships apply for a short or open-end CPW stub with any dimensions. Thus, it is enough to model two different stub lengths, from which the characteristics of other lengths can be derived.

V. Conclusions

A space-domain integral equation method solved by the method of moments in conjunction with simple transmission line theory was applied to analyze CPW circuit elements useful for band-pass and band-stop filters. An experimental setup to measure the scattering parameters of those structures has been described. The agreement between the theoretical results and the experimental data was very good; thus, the validity of both results is verified. Lumped element equivalent circuits were proposed to model the above circuit elements, and closed-form expressions to compute the values of the capacitances and inductances were given as functions of stub length.

Appendix

As shown in Fig. 12, a typical CPW discontinuity problem is reduced to deriving the dyadic Green's function in both regions directly above and below the slots. The transmission line theory is used to transform the surrounding layers into impedance boundaries. Using the equivalence principle, the problem is divided into four subproblems (as shown in Fig. 12), where the fields in both regions due to magnetic currents in the y and z directions have to be obtained. After this has been accomplished, the continuity of the tangential fields at the interface is used to arrive at the integral equation. The main steps in the derivation of the fields arising from an infinitesimal z-directed magnetic current inside a cavity (with impedance boundary top side) will be presented here (see Fig. 13).

In the derivations, the following vector potentials for the LSM and LSE modes are assumed:

$$A = \hat{a}_x \psi \qquad F = \hat{a}_x \phi. \qquad (A1)$$

By using Maxwell's equations along with

$$H = \frac{1}{\mu} \nabla \times A \qquad (A2)$$

$$E = -\frac{1}{\epsilon} \nabla \times F \qquad (A3)$$

one can obtain the field components in terms of the magnetic and electric vector potentials.

The differential equations for A and F are solved in view of the pertinent boundary conditions to give the unknown field components. The boundary conditions considered for the solution of this problem are listed below (see Fig. 13, where the magnetic current dipole is raised

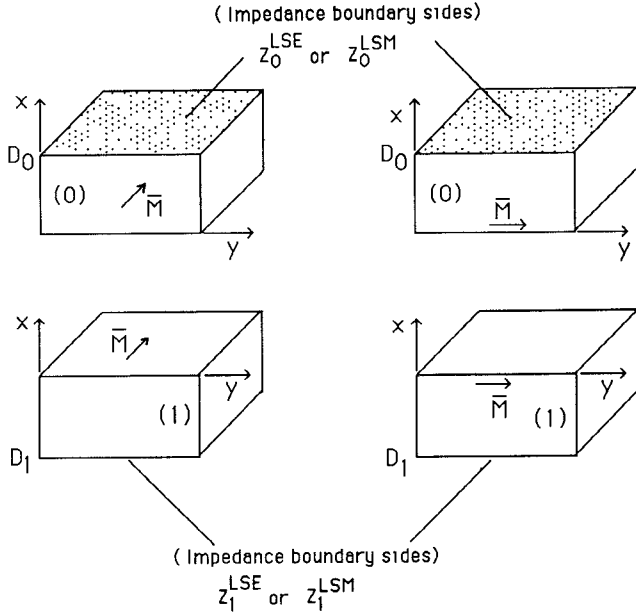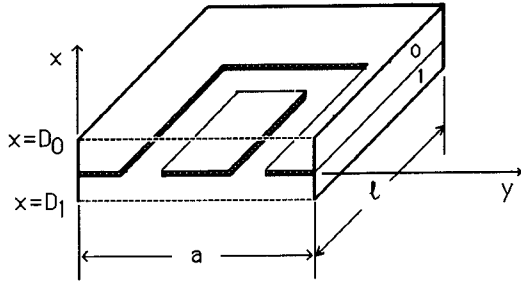Fig. 13. A z-directed magnetic dipole inside a cavity with an impedance boundary top side.

Fig. 12. A typical one-port CPW discontinuity where four subproblems are obtained using the equivalence principle. (All the sides excluding the impedance boundaries are assumed perfectly conducting.)

to simplify the application of the boundary conditions):

$$E_z^I = E_z^{II} \quad \text{at} \quad x = x' \tag{A4}$$

$$H_y^I = H_y^{II} \quad \text{at} \quad x = x' \tag{A5}$$

$$H_z^I = H_z^{II} \quad \text{at} \quad x = x' \tag{A6}$$

$$\left(\frac{E_y^I}{H_z^I} \right)^{LSE} = Z_0^{LSE} \quad \text{at} \quad x = D_0 \tag{A7}$$

$$\left(\frac{E_y^I}{H_z^I} \right)^{LSM} = Z_0^{LSM} \quad \text{at} \quad x = D_0 \tag{A8}$$

$$E_y^{II} - E_y^I = \delta(x - x')\delta(y - y')\delta(z - z'). \tag{A9}$$

In (A4)–(A9), D_0 is the thickness of the layer directly above the slot apertures. Z_0^{LSE} and Z_0^{LSM} are the LSE and LSM impedances seen at the interface $x = D_0$. For the structures considered here (Fig. 3), $Z_0^{LSE} = Z_0^{LSM} = 0$ since perfect conductors are assumed. Solving (A4)–(A9), the fields in the region directly above the slot aperture caused by a z-directed magnetic dipole are obtained. In the same manner the fields due to a y-directed magnetic dipole can be derived.
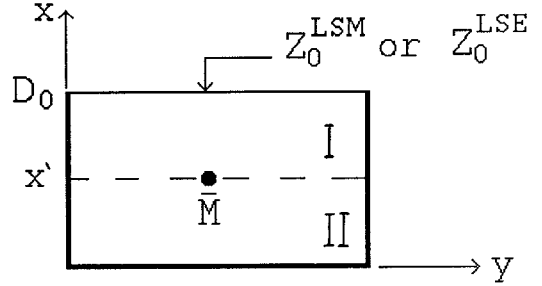
The components of the dyadic Green's function for the coplanar waveguide problem are given by the following expressions:

$$G_{yy}^{(0)}(\bar{r}/\bar{r}') = \sum_{m=0}^{MSTOP} \sum_{n=0}^{NSTOP} \frac{2e_n}{al} \frac{1}{k_{x_0}^2 - k_0^2} \left[k_y^2 P_0 + k_z^2 Q_0 \right]$$
$$\cdot \sin(k_y y') \cos(k_z z') \sin(k_y y) \cos(k_z z) \tag{A10}$$

$$G_{zy}^{(0)}(\bar{r}/\bar{r}') = \sum_{m=0}^{MSTOP} \sum_{n=0}^{NSTOP} \frac{2e_n}{al} \frac{k_y k_z}{k_{x_0}^2 - k_0^2} \cdot [P_0 - Q_0]$$
$$\cdot \sin(k_y y') \cos(k_z z') \cos(k_y y) \sin(k_z z) \tag{A11}$$

$$G_{yz}^{(0)}(\bar{r}/\bar{r}') = \sum_{m=0}^{MSTOP} \sum_{n=0}^{NSTOP} \frac{2e_n}{al} \frac{k_y k_z}{k_{x_0}^2 - k_0^2} [P_0 - Q_0]$$
$$\cdot \cos(k_y y') \sin(k_z z') \sin(k_y y) \cos(k_z z) \tag{A12}$$

$$G_{zz}^{(0)}(\bar{r}/\bar{r}') = \sum_{m=0}^{MSTOP} \sum_{n=0}^{NSTOP} \frac{2e_m}{al} \frac{1}{k_{x_0}^2 - k_0^2} \left[k_z^2 P_0 + k_y^2 Q_0 \right]$$
$$\cdot \cos(k_y y') \sin(k_z z') \cos(k_y y) \sin(k_z z) \tag{A13}$$

where

$$P_0 = \left(\frac{k_{x_0}}{\omega \mu_0} \right) \frac{\omega \mu_0 + jk_{x_0} Z_0^{LSE} \tan(k_{x_0} D_0)}{k_{x_0} Z_0^{LSE} + j\omega \mu_0 \tan(k_{x_0} D_0)} \tag{A14}$$

$$Q_0 = \left(\frac{\omega \epsilon_0}{k_{x_0}} \right) \frac{k_{x_0} + j\omega \epsilon_0 Z_0^{LSM} \tan(k_{x_0} D_0)}{\omega \epsilon_0 Z_0^{LSM} + jk_{x_0} \tan(k_{x_0} D_0)} \tag{A15}$$

$$e_n = 1, \quad n = 0$$
$$= 2, \quad n \neq 0 \tag{A16}$$

$$e_m = 1, \quad m = 0$$
$$= 2, \quad m \neq 0 \tag{A17}$$

$$k_y = \frac{m\pi}{a} \tag{A18}$$

$$k_z = \frac{n\pi}{l} \tag{A19}$$

$$k_0^2 = \omega^2 \mu_0 \epsilon_0 \tag{A20}$$

$$k_0^2 = k_{x_0}^2 + k_y^2 + k_z^2. \tag{A21}$$

In the above expressions, a and l are the width and length of the cavity, respectively, and $G_{ij}^{(0)}$ denotes the magnetic field $H_i^{(0)}$ radiated at $x = 0$ by an infinitesimal magnetic dipole M_j located at $x' = 0$ $(i, j = y, z)$.

The components of $\overline{\overline{G}}_1^h$ are essentially the same as in (A10)–(A21) with the following changes:

$$Z_0^{LSE} \to Z_1^{LSE}$$
$$Z_0^{LSM} \to Z_1^{LSM}$$
$$D_0 \to D_1$$
$$e_n, e_m \to -e_n, -e_m$$
$$k_0 \to k_1$$
$$\mu_0, \epsilon_0 \to \mu_1, \epsilon_1 \qquad (A22)$$

where Z_1^{LSE} and Z_1^{LSM} are the LSE and LSM impedances seen at the interface $x = D_1$.

References

[1] M. Houdart, "Coplanar lines: Application to broadband microwave integrated circuits," in *Proc. 6th European Microwave Conf.* (Rome), 1976, pp. 49–53.

[2] R. A. Pucel, "Design considerations for monolithic microwave circuits," *IEEE Trans. Microwave Theory Tech.*, vol. MTT-29, pp. 513–534, June 1981.

[3] R. W. Jackson, "Considerations in the use of coplanar waveguide for millimeter wave integrated circuits," *IEEE Trans. Microwave Theory Tech.*, vol. MTT-34, pp. 1450–1456, Dec. 1986.

[4] M. Riaziat, E. Par, G. Zdasiuk, S. Bandy, and M. Glenn, "Monolithic millimeter wave CPW circuits," in *1989 IEEE MTT-S Int. Microwave Symp. Dig.* (Long Beach, CA), pp. 525–528.

[5] T. Hirota, Y. Tarusawa, and H. Ogawa, "Uniplanar MMIC hybrids —A Proposed new MMIC structure," *IEEE Trans. Microwave Theory Tech.*, vol. MTT-35, pp. 576–581, June 1987.

[6] M. Riaziat, R. Majidi-Ahi, and I. Feng, "Propagation modes and dispersion characteristics of coplanar waveguides," *IEEE Trans. Microwave Theory Tech.*, vol. 38, pp. 245–251, Mar. 1990.

[7] K. C. Gupta, R. Garge and I. J. Bahl, *Microstrip Lines and Slotlines.* Dedham, MA: Artech House, 1979.

[8] R. N. Simons and G. E. Ponchak, "Modeling of some coplanar waveguide discontinuities," *IEEE Trans. Microwave Theory Tech.*, vol. 36, pp. 1796–1803, Dec. 1988.

[9] N. H. Koster, S. Koblowski, R. Bertenburg, S. Heinen, and I. Wolff, "Investigation of air bridges used for MMICs in CPW technique," in *Proc. 19th European Microwave Conf.* (London), Sept. 1989, pp. 666–671.

[10] G. Kibuuka, R. Bertenburg, M. Naghed and I. Wolff, "Coplanar lumped elements and their application in filters on ceramic and gallium arsenide substrates," in *Proc. 19th European Microwave Conf.* (London), Sept. 1989, pp. 656–661.

[11] C. W. Kuo and T. Itoh, "Characterization of the coplanar waveguide step discontinuity using the transverse resonance method," in *Proc. 19th European Microwave Conf.* (London), Sept. 1989, pp. 662–665.

[12] R. W. Jackson, "Mode conversion at discontinuities in finite-width conductor-backed coplanar waveguide," *IEEE Trans. Microwave Theory Tech.*, vol. 37, pp. 1582–1589, Oct. 1989.

[13] G. Matthaei, L. Young and E. Jones, *Microwave Filters, Impedance-Matching Networks, and Coupling Structures.* Dedham, MA: Artech House, 1980.

[14] D. F. Williams and S. E. Schwarz, "Design and performance of coplanar waveguide band-pass filters," *IEEE Trans. Microwave Theory Tech.*, vol. MTT-31, pp. 558–566, July 1983.

[15] G. E. Ponchak and R. N. Simons, "Channelized coplanar waveguide PIN-diode switches," in *Proc. 19th European Microwave Conf.* (London), 1989, pp. 489–494.

[16] R. F. Harrington, *Field Computation by Moment Methods.* New York: Macmillan, 1968.

[17] N. I. Dib and P. B. Katehi, "Modeling of shielded CPW discontinuities using the space domain integral equation method (SDIE)," *J. Electromagn. Waves and Appl.*, to be published.

[18] N. I. Dib, P. B. Katehi, G. E. Ponchak, and R. N. Simons, "Coplanar waveguide discontinuities for p-i-n diode switches and filter applications," in *1990 IEEE MTT-S Int. Microwave Symp. Dig.*, May 1990, pp. 399–402.

[19] A. W. Glisson and D. R. Wilton, "Simple and efficient numerical methods for problems of electromagnetic radiation and scattering from surfaces," *IEEE Trans. Antennas Propagat.*, vol. AP-28, pp. 593–603, Sept. 1980.

[20] W. P. Harokopus and P. B. Katehi, "Characterization of microstrip discontinuities on multilayer dielectric substrates including radiation losses," *IEEE Trans. Microwave Theory Tech.*, vol. 37, pp. 2058–2065, Dec. 1989.

[21] P. B. Katehi, "A generalized method for the evaluation of mutual coupling in microstrip arrays," *IEEE Trans. Antennas Propagat.*, vol. AP-35, pp. 125–133, Feb. 1987.

[22] R. E. Stegens, "Coplanar waveguide FET amplifiers for satellite communications systems," *Comsat Tech. Rev.*, vol. 9, pp. 255–267, spring 1979.
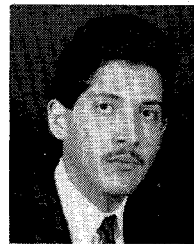
Nihad I. Dib (S'89) was born in Palestine in May 1964. He received the B.S. and M.S. degrees in electrical engineering from Kuwait University in 1985 and 1987, respectively.

He worked as a Laboratory Engineer in the Department of Electrical Engineering and Computer Science at Kuwait University for two years. He has been with the Radiation Laboratory, University of Michigan, since September 1988. He is currently working toward the Ph.D. degree. His research interests include numerical techniques applied to electromagnetic problems and planar discontinuities.

Linda P. B. Katehi (S'81–M'84–SM'89) received the B.S.E.E. degree from the National Technical University of Athens, Greece, in 1977 and the M.S.E.E. and Ph.D. degrees from the University of California, Los Angeles, in 1981 and 1984, respectively.

In September 1984 she joined the faculty of the Department of Electrical Engineering and Computer Science at the University of Michigan, Ann Arbor. Since then, she has been involved in the modeling and computer-aided design of millimeter- and near-millimeter-wave monolithic circuits and antennas.

In 1984 Dr. Katehi received the W. P. King Award and in 1985 the S. A. Schelkunoff Award from the Antennas and Propagation Society. In 1987 she received an NSF Presidential Young Investigator Award and an URSI Young Scientist Fellowship. She is a member of Sigma Xi.
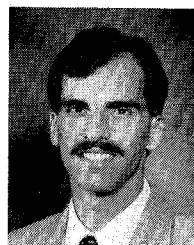
George E. Ponchak (S'82–M'90) received the B.E.E. degree from Cleveland State University, Cleveland, OH, in 1983 and the M.S.E.E. degree from Case Western Reserve University, Cleveland, OH, in 1987.

He joined the NASA Lewis Research Center, Cleveland, OH, in July 1983 as a member of the Space Communications Division. Since joining NASA he has been engaged in research in solid-state technology development, transmission lines, and monolithic microwave integrated circuits (MMIC's). He is currently at the University of Michigan pursuing the Ph.D. degree.
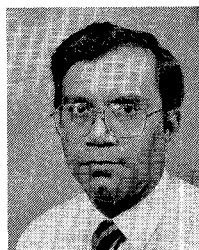
Rainee N. Simons (S'76–M'80–SM'89) received the B.E. degree in electronics and communications from Mysore University in 1972, the M. Tech. degree in electronics and communications from the Indian Institute of Technology, Kharagpur, in 1974, and the Ph.D. degree in electrical engineering from the Indian Institute of Technology, New Delhi, in 1983.

He is currently a Resident Research Associate in the Solid State Technology Branch of the Space Electronics Division, NASA Lewis Research Center, Cleveland, OH. From 1985 to 1987 he was a National Research Council Research Associate and carried out investigations on the direct optical control of GaAs microwave semiconductor devices and circuits. Prior to this, he was a Senior Scientific Officer at the Indian Institute of Technology, New Delhi, where he worked on finline components for millimeter-wave applications and also on toroidal latching ferrite phase shifters for phased arrays. His current research interests include the analysis and modeling of GaAs microwave semiconductor devices and circuits in MMIC's, optical control, and high-temperature superconductivity.

Dr. Simons held the post of IEEE Student Chapter Chairman at the Indian Institute of Technology, New Delhi, from 1978 to 1979. He also held the posts of IEEE Indian Council ED/MTT Society Chapter (New Delhi) Joint Secretary, Executive Committee Member, and Vice Chairman during the years 1982, 1983, and 1984, respectively. He is the author of *Optical Control of Microwave Devices* (Artech House, 1990).